

RESEARCH

Open Access



Preoperative prediction of microvascular invasion and relapse-free survival in hepatocellular Carcinoma ≥ 3 cm using CT radiomics: Development and external validation

Hua Zhong^{1†}, Yan Zhang^{2†}, Guanbin Zhu¹, Xiaoli Zheng¹, Jinan Wang¹, Jianghe Kang¹, Ziyang Lin^{1*} and Xin Yue^{1*}

Abstract

Objective To preoperatively predict microvascular invasion (MVI) and relapse-free survival (RFS) in hepatocellular carcinoma (HCC) ≥ 3 cm by constructing and externally validating a combined radiomics model using preoperative enhanced CT images.

Methods This retrospective study recruited adults who underwent surgical resection between September 2016 and August 2020 in our hospital with pathologic confirmation of HCC ≥ 3 cm and MVI status. For external validation, adults who underwent surgical resection between September 2020 and August 2021 in our hospital were included. Histopathology was the reference standard. The HCC area was segmented on the arterial and portal venous phase CT images to develop a CT radiomics model. A combined model was developed using selected radiomics features, demographic information, laboratory index and radiological features. Analysis of variance and support vector machine were used as features selector and classifier. Receiver operating characteristic (ROC) curves, calibration curves and decision curve analysis (DCA) were used to evaluate models' performance. The Kaplan-Meier method and log-rank test were used to evaluate the predictive value for RFS.

Results A total of 202 patients were finally enrolled (median age, 59 years, 173 male). Thirteen and 24 features were selected for the CT radiomics model and the combined model, and the area under the ROC curves (AUC) were 0.752 (95 %CI 0.615, 0.889) and 0.890 (95 %CI 0.794, 0.985) in the external validation set, respectively. Calibration curves and DCA showed a higher net clinical benefit of the combined model. The high-risk group ($P < 0.001$) was an independent predictor for RFS.

[†]Yan Zhang and Hua Zhong contributed equally to this work.

*Correspondence:

Ziyang Lin

linzy1224@163.com

Xin Yue

yuexin7504@163.com

Full list of author information is available at the end of the article



Conclusions The combined model showed high accuracy for preoperatively predicting MVI and RFS in HCC ≥ 3 cm.

Keywords Microvascular invasion, Hepatocellular carcinoma, Radiomics, CT, Relapse-free survival

Introduction

Hepatocellular carcinoma (HCC) is one of the leading cancers with rising prevalence, high mortality and poor clinical outcome all over the world [1, 2]. Microvascular invasion (MVI), which refers to the presence of clusters of cancer cells in blood vessels with endothelial cell linings, commonly most pronounced in the branches of the peri-neoplastic portal vein (including the intra-capsular blood vessels) under microscope [3], is an independent risk factor for poor prognosis in patients with HCC [4]. Different treatment strategies are recommended for different MVI status [5]. Moreover, tumor size ≥ 3 cm is independently associated with increased HCC recurrence risk [6]. Therefore, accurate preoperative prediction of MVI in HCC ≥ 3 cm is of great importance for treatment and prognosis. Although there are a large number of studies paying close attention to the early recurrence of HCC, how much difference of relapse-free survival (RFS) between MVI (+) and MVI (-) in HCC ≥ 3 cm is not clear.

Dynamic contrast-enhanced CT is one of the first-choice imaging methods for clinical diagnosing and staging of HCC [3]. Several studies have identified several imaging features associated with MVI, such as irregular shape, infiltrative border, incomplete capsule, peritumoral enhancement, internal arteries, absence of hypodense halo and tumor-liver difference [7–11]. Also, radiomics, which refers to the high-throughput extraction of quantitative features from images that results in the conversion of images into mineable data and the subsequent analysis of these data for decision support [12], has been attempted to predict MVI based on preoperative images [13].

Machine learning (ML) is a branch of data science that enables computers to learn from existing “training” data without explicit programming, which can be used at any step of radiomics [14]. Support vector machines (SVM) is a classifier which maps nonlinear data into a higher dimensional space and generates a hyperplane that separates the classes. Its high generalization ability makes it to be used in many fields of classification successfully [15].

We aimed to preoperatively predict MVI, intrahepatic recurrence-free survival and extrahepatic metastasis-free survival in HCC ≥ 3 cm by constructing and externally validating combined radiomics model using preoperative enhanced CT images.

Materials and methods

Patients

Ethical approval was obtained for this retrospective study from Institutional Review Board of Zhongshan Hospital

of Xiamen University [2022(212)] and the need to obtain informed consent was waived. The study has been performed in accordance with the Declaration of Helsinki. For model development, 240 consecutive patients who underwent surgical resection between September 2016 and August 2020 in our hospital with pathologic confirmation of hepatocellular carcinoma and MVI status were included in this study. The exclusion criteria were as follows: (1) Underwent other treatments before enhanced CT ($n=31$); (2) lack of enhanced CT within one month before surgery ($n=18$); and (3) with tumor diameter <3 cm ($n=38$). Patients were randomly divided into two separate cohorts at a ratio of 7:3. Thus the training set included 108 patients and the test set included 45 patients. For temporal external validation, 93 consecutive patients who underwent surgical resection between September 2020 and August 2021 in our hospital with pathologic confirmation of hepatocellular carcinoma and MVI status were included. The exclusion criteria were as follows: (1) Underwent other treatments before enhanced CT ($n=22$); (2) lack of enhanced CT within one month before surgery ($n=7$); and (3) with tumor diameter <3 cm ($n=15$). Thus, a total of 202 patients were finally enrolled (173 men and 29 women; median age, 59 years) (Fig. 1). The demographic information, laboratory tests, histopathological diagnosis and follow-up information were obtained from the electronic medical records, including age, sex, α -fetoprotein (AFP), prothrombin time (PT), alanine transaminase (ALT), aspartate transaminase (AST) and hepatitis B virus DNA (HBV DNA). CT images were retrieved from the picture archiving and communication system.

CT protocols

The CT was performed using Philips Iqon-Spectral CT (Netherlands), Philips Ingenuity CT (Netherlands), GE Lightspeed VCT (the United States), GE Revolution (the United States), Siemens Somatom Definition Flash (Germany) or Siemens Definition AS (Germany). The following CT scanning parameters were used: 120 kV, 100–300 effective mA, 2.5–5 mm thickness. The non-enhanced phase images were obtained before administration of the contrast agent. Enhanced imaging was performed after administration of 90–100 ml of non-ionic contrast medium at a rate of 3–3.5 ml/s. Arterial phase, portal venous and equilibrium phase images were obtained 30, 65 and 120 s after administration of the contrast material, respectively.

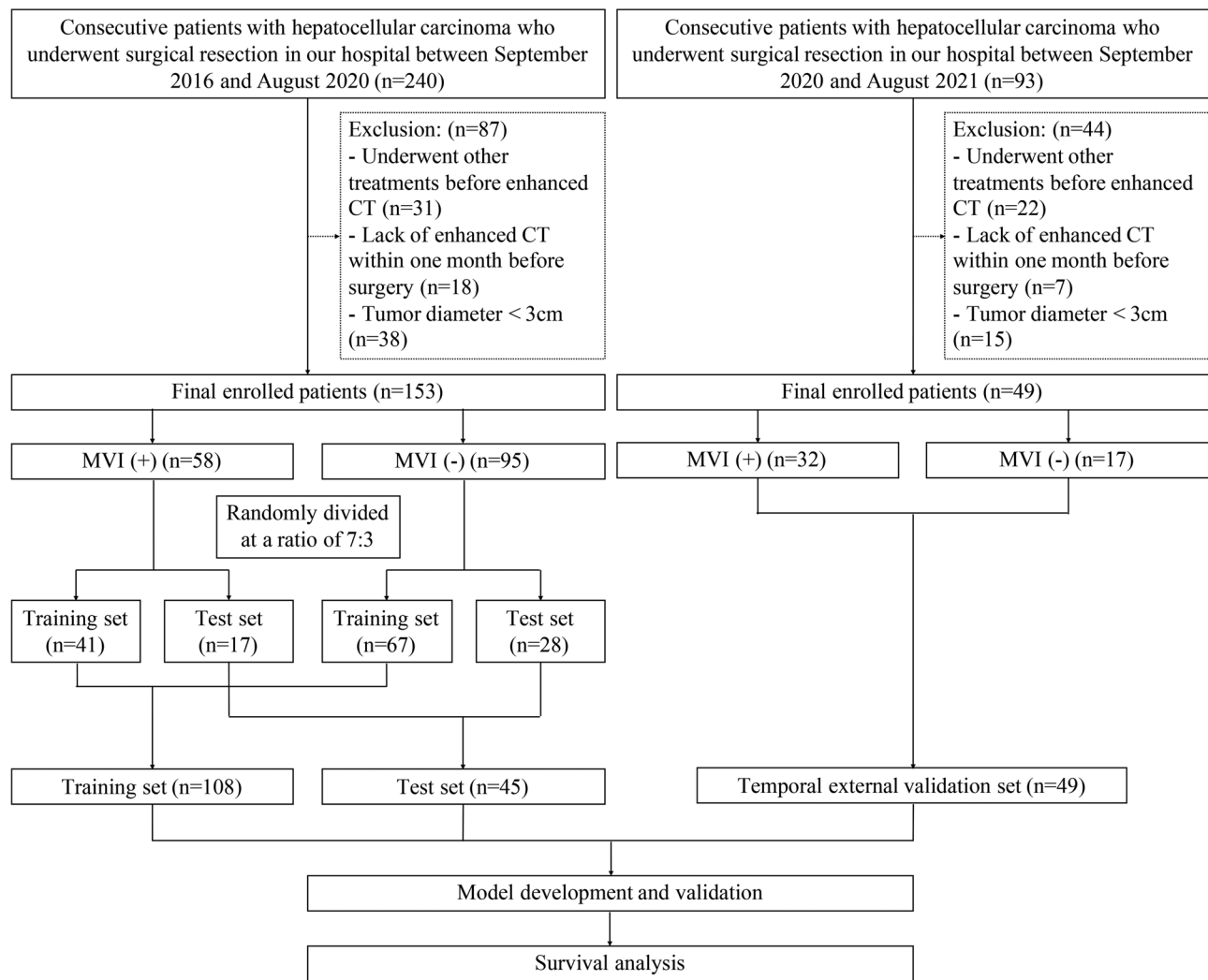


Fig. 1 Flowchart for patient enrolment

Radiological features

The radiological features included diameter, shape, border, capsule, necrosis, peritumoral enhancement, internal arteries, hypodense halo and tumor-liver difference [16]. “Internal arteries” is the persistence of discrete arterial enhancement within the tumor in the venous phase of imaging [16]. “Hypodense halo” is a rim of hypoattenuation partially or completely circumscribing the tumor [13]. “Tumor-liver difference” is a focal or circumferential sharp transition in attenuation between the tumor and the adjacent liver parenchyma in the absence of a hypodense halo [11]. Two radiologists, with 4 and 6 years of experience respectively, who were blinded to the clinicopathologic data, evaluated the radiological features. And a senior radiologist with 20 years of experience confirmed the radiological features. The inter-observer reproducibility was measured in the first 100 patients by two radiologists.

Pathological diagnosis

Histopathology is the reference standard for MVI diagnosis. According to the Evidence-based Practice Guidelines for the Standardized Pathological Diagnosis of Primary Liver Cancer in China (2015 Update) [17], M0 was defined as no MVI; M1 was defined as MVI of <5 and at ≤1 cm away from the adjacent liver tissues; and M2 was defined as MVI of >5 or at >1 cm away from the adjacent liver tissues. Patients with M0 were grouped into MVI (-) group and patients with M1 and M2 were grouped into MVI (+) group.

Follow-up

Four patients were excluded due to lack of follow-ups for the follow-up cohort. Patients underwent routine follow-up with dynamic CT or MRI every 2–3 months within 6 months after treatment and every 3–6 months after 6 months. RFS was defined as the interval between the date of surgery and the detected recurrence or last

follow-up [18]. Patients were censored at the time of the last follow-up, or the study end date of November 15, 2023.

Image segmentation and radiomics feature extraction

ITK-SNAP software (version 3.6.0; <https://www.itksnap.org>) was used for the 3D segmentation [19]. Two radiologists, with 4 and 6 years of experience respectively, who were blinded to the clinicopathologic data, manually delineated the tumors volume of interest (VOI) on the arterial phase and portal venous phase CT images. And the segmentations were confirmed by a senior radiologist with 20 years of experience, and were revised, if necessary (Fig. 2). The intraclass correlation coefficient was used to determine the inter- and intra- observer reproducibility using the first 30 lesions. Radiomics features were extracted from the VOI of arterial phase and portal venous phase CT images using FeAture Explorer [20]. Features were standardized using Z-score normalization and were reduced using Pearson correlation coefficient value.

Model development, validation and evaluation

We up-sampled by repeating random cases to remove the unbalance of the groups. The optimal radiomics features were chosen using the analysis of variance (ANOVA), and SVM was used as the classifier [20]. A radiomics

model was established using radiomics features, and a combined model was established using demographic information, laboratory index and radiological features and ANOVA-SVM-selected radiomics features. Cross validation with 5-fold on the training set was used, and an external validation set was used for external validation of model performance. Patients were classified into a high-risk group (rad-score ≥ 0.5) and a low-risk group (rad-score < 0.5) of MVI. Receiver operating characteristic (ROC) curve analysis, calibration curves and decision curve analysis (DCA) were used for evaluating the performance of each model. And the area under the ROC curve (AUC), accuracy, sensitivity, specificity, positive predictive value (PPV) and negative predictive value (NPV) were calculated.

Statistical analysis

The statistical analyses were performed with SPSS version 26.0 (IBM Corp., Armonk, NY, USA) and STATA version 15. Continuous variables that do not follow a normal distribution were summarized as median (interquartile range), and categorical variables were summarized using counts (percentage). Mann-Whitney U tests and chi-square tests were used as appropriate for univariate analyses. The DeLong test was used to compare the ROC of the two models. The Kaplan-Meier method was used to generate survival curves, and the log-rank test

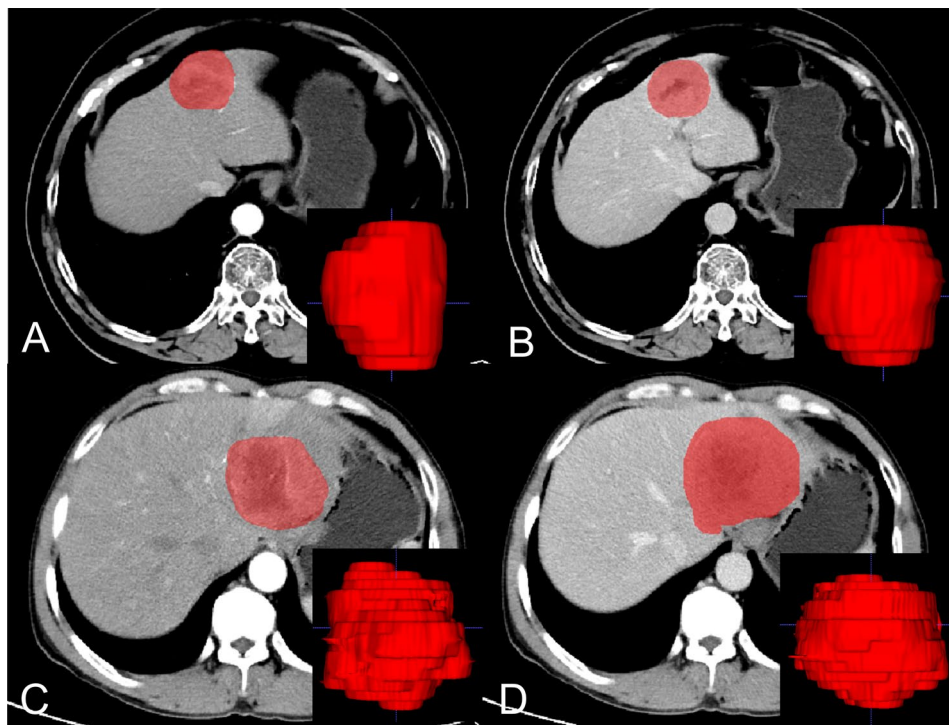


Fig. 2 CT images and segmentations in patients with hepatocellular carcinoma. Volume of interest (VOI) of arterial phase (A) and portal venous phase (B) in hepatocellular carcinoma (HCC) without MVI, and the corresponding volume-rendering images. VOI of arterial phase (C) and portal venous phase (D) in HCC with MVI, and the corresponding volume-rendering images

and Breslow test were performed. A two-sided $p < 0.05$ was considered statistically significant.

Results

Patient characteristics

The characteristics of the patients in the training, the test set and the external validation set are summarised in Table 1. The rates of MVI (+) were 38.0 % (41 of 108), 37.8 % (17 of 45) and 65.3 % (32 of 49) in the training, the test and the external validation set, respectively. There were no significant differences in age, sex, diameter, AFP, PT, ALT or AST between the sets ($p = 0.363-0.822$).

Development of the CT radiomics model

From the CT images, 1888 radiomics features were initially extracted. Thirteen radiomics features were finally selected as follows: A_original_gldm_GrayLevelNonUniformity, A_original_glszm_GrayLevelNonUniformity, A_square_glszm_LargeAreaLowGrayLevelEmphasis, A_wavelet-HLL_glszm_GrayLevelNonUniformity, A_wavelet-HLL_glszm_SzrZoneNonUniformity, A_wavelet-HLL_glszm_SmallAreaEmphasis, A_wavelet-HLL_glszm_SmallAreaLowGrayLevelEmphasis, A_wavelet-LLL_gldm_GrayLevelNonUniformity, V_original_gldm_GrayLevelNonUniformity, V_original_glrmlm_GrayLevelNonUniformity, V_wavelet-HLL_glcm_ClusterShade, V_wavelet-LLH_gldm_DependenceNonUniformity, V_wavelet-LLL_gldm_GrayLevelNonUniformity. The rad-score was related to MVI (+) in the training set ($p < 0.001$) and the external validation set ($p = 0.043$). The AUCs of the training set, the test set and the external validation set were 0.780 (95 %CI 0.687, 0.871), 0.761 (95 %CI 0.600, 0.921) and 0.752 (95 %CI 0.615, 0.889), respectively.

Development of the combined model

The inter-observer reproducibility was moderate to good, with a Kappa of 0.450–0.741 ($p < 0.001$). Twenty-four features were selected for the combined model, with 13 radiomics features, 3 laboratory feature and 8 radiological features (Table 2). The rad-score was related to MVI (+) in the training set, the test set and the external validation set ($p < 0.001$). The AUCs of the training set, the test set and the external validation set were 0.914 (95 %CI 0.854, 0.973), 0.878 (95 %CI 0.758, 0.999) and 0.890 (95 %CI 0.794, 0.985), respectively. The accuracy, sensitivity, specificity, PPV and NPV are listed in Table 3.

Comparison of the predictive performance of the models

A comparison of the models is provided in Fig. 3. The combined model had a higher AUC than the CT radiomics model ($p < 0.001$). The calibration curves and the DCA indicated that the combined model provided a higher net clinical benefit than the CT radiomics model.

Table 1 Demographic and clinical characteristics of patients in the training set, the test set and the external validation set

	Total	Training		Test		External Validation		P	P*					
		All	MVI (+)	MVI (-)	All	MVI (+)	MVI (-)			All	MVI (+)	MVI (-)		
Patients (%)	202(100%)	108(53.5%)	41(38.0%)	67(62.0%)	-	45(22.3%)	17(37.8%)	28(62.2%)	49(24.3%)	32(65.3%)	17(34.7%)	-	-	
Age, years	59(19)	60(19)	58(16)	61(19)	0.394	59(15)	59(13)	59(17)	0.482	57(20)	57(18)	62(23)	0.475	0.653
Sex, male (%)	173(85.6%)	90(83.3%)	36(87.8%)	54(80.6%)	0.329	39(86.7%)	15(88.2%)	24(85.7%)	0.809	44(89.8%)	28(87.5%)	16(94.1%)	0.466	0.550
Diameter, mm	58(50)	58(56)	70(65)	49(47)	0.003	55(47)	82(74)	43(38)	0.006	64(47)	80.5(68)	50(23)	0.001	0.363
AFP, ng/mL	38.15(948.74)	34.23(799.52)	105.2(9815.35)	8.48(364.17)	0.004	48.72(1701.43)	217.8(5056.10)	22.95(703.28)	0.096	39.1(988.85)	207.75(1170.93)	8.5(90.65)	0.037	0.755
PT, sec	11.8(1.3)	11.8(1.3)	12(1.3)	11.6(1.4)	0.317	11.8(1.5)	12(1)	11.7(1.5)	0.281	11.8(1.5)	12.1(1.5)	11.6(1.2)	0.012	0.462
ALT, U/L	34.1(31.3)	33.3(31.3)	31(44.2)	34.2(22)	0.822	35.9(31.9)	37.8(44.3)	33.8(25.5)	0.743	34.1(32.8)	34.55(24.8)	32.3(46.8)	0.508	0.731
AST, U/L	37.5(35.9)	38.1(36.2)	43.3(45.0)	36.6(30.9)	0.264	35.8(37.6)	39.3(38.2)	32.1(34.4)	0.242	37.9(31.5)	40.45(33.6)	36.4(28.7)	0.383	0.822

Note: Unless otherwise specified, data are summarized as median, with interquartile range in parentheses

Abbreviations: AFP, α -fetoprotein; PT, prothrombin time; ALT, alanine transaminase; AST, aspartate transaminase.

* The p value reflects the comparison between the training set, the test set and the external validation set.

Table 2 Twenty-four features in the combined model

Feature	MVI (-)	MVI (+)	<i>P</i> *
A_original_gldm_GrayLevelNonUniformity	12326.1	46972.6	<0.001
A_original_glszm_GrayLevelNonUniformity	61.0	194.4	<0.001
A_square_glszm_LargeAreaLowGrayLevelEmphasis	3.9*10 ⁸	5.5*10 ⁹	<0.001
A_wavelet-HHL_glszm_GrayLevelNonUniformity	4.1	6.4	<0.001
A_wavelet-HHL_glszm_SizeZoneNonUniformity	2.1	4.0	<0.001
A_wavelet-HHL_glszm_SmallAreaEmphasis	0.46	0.55	<0.001
A_wavelet-HHL_glszm_SmallAreaLowGrayLevelEmphasis	0.27	0.34	<0.001
A_wavelet-LLL_gldm_GrayLevelNonUniformity	6402	24981	<0.001
V_original_gldm_GrayLevelNonUniformity	12823	46259	<0.001
V_original_glrIm_GrayLevelNonUniformity	3542	9498	<0.001
V_wavelet-HHL_glcM_ClusterShade	4.5*10 ⁻⁴	-1.5*10 ⁻⁴	0.005
V_wavelet-LLH_gldm_DependenceNonUniformity	1305	4399	<0.001
V_wavelet-LLL_gldm_GrayLevelNonUniformity	7035	22552	<0.001
Diameter	49	80	<0.001
Shape, irregular, %	55	81	<0.001
Border, ill-defined, %	27	40	0.047
Capsule, without, %	10	39	<0.001
Peritumoral Enhancement, %	8	29	<0.001
Internal Arteries, %	18	61	<0.001
Hypodense Halo, %	25	41	0.015
Tumor-Liver Difference, %	12	31	<0.001
AFP	10	150	<0.001
ALB	41	39	0.002
HBV_DNA	6290	651	0.002

Note: Unless otherwise specified, data are summarized as median

Abbreviations: AFP, α -fetoprotein; ALB, albumin; HBV_DNA, hepatitis B virus DNA

*The *p* value reflects the comparison between the MVI (+) group and MVI (-) group

Predictive value of the combined model for postoperative recurrence

The median survival time was 746 days. The median follow-up time was 664 days. Among the 198 included patients, there were 85 (42.9%) patients with recurrence, including 50 (25.3%) with intrahepatic recurrence, 12 (6.1%) with extrahepatic metastasis and 23 (11.6%) with both intrahepatic recurrence and extrahepatic

metastasis. The 1-, 2- and 3-year RFS rates were 64.2%, 49.8% and 41.9%, respectively. MVI (+) group (1-, 2- and 3-year RFS rates of 57.7%, 32.9% and 20.6%, respectively) showed a shorter RFS than MVI (-) group (1-, 2- and 3-year RFS rates of 69.3%, 59.6% and 54.7%, respectively) ($P=0.001$) (Fig. 4).

There was no statistically significant difference of RFS between MVI (+) group and high-risk group ($P=0.807$), or MVI (-) group and low-risk group ($P=0.948$) (Fig. 4). The high-risk group (HR, 2.055, 95% CI: 1.341, 3.149, $P<0.001$) was an independent predictor for RFS after surgical resection. High-risk group showed a shorter RFS (1- and 2-year RFS rates of 52.5% and 32.6%, respectively) than low-risk group (1- and 2-year RFS rates of 71.7% and 61.3%, respectively) ($P<0.001$). Moreover, high-risk group (1- and 2-year intrahepatic recurrence-free survival rates of 58.6% and 48.5%, 1- and 2-year extrahepatic metastasis-free survival rates of 74.8% and 56.1%) showed a shorter intrahepatic recurrence-free survival ($P=0.049$) and extrahepatic metastasis-free survival ($P<0.001$) than low-risk group (1- and 2-year intrahepatic recurrence-free survival rates of 73.6% and 63.2%, 1- and 2-year extrahepatic metastasis-free survival rates of 92.8% and 91.0%).

Discussion

In this study, we developed and validated a CT radiomics model and a combined model based on ML to preoperatively predict MVI and RFS in patients with HCC ≥ 3 cm. The results showed that both models had good to excellent predictive performance. In particular, a high rad-score of MVI in the combined model was associated with shorter RFS, indicating its potential clinical application.

Although rate of MVI (+) in the external validation set was significantly different from that in the training and the test set, the combined model shows good performance for MVI prediction in the external validation set, suggesting its strong ability in generalization. There have been several studies that preoperatively predict MVI in HCC using contrast-enhanced CT or contrast-enhanced MRI. These studies included HCC of any size, and the AUCs of the combined radiomics model in the external validation set were 0.756–0.840 [13, 21–23]. Compared to the above studies, the combined model in our study which contains demographic information, laboratory index, radiological features and ANOVA-SVM-selected radiomics features shows better MVI prediction

Table 3 Performance of the combined model in the training set, the test set and the external validation set

Set	AUC	Accuracy	Sensitivity	Specificity	PPV	NPV
Training set	0.914(0.854,0.973)	0.843(0.762,0.899)	0.829(0.687,0.915)	0.851(0.747,0.917)	0.773(0.630,0.872)	0.891(0.791,0.946)
Test set	0.878(0.758,0.999)	0.800(0.662,0.891)	0.765(0.527,0.904)	0.821(0.644,0.921)	0.722(0.491,0.875)	0.852(0.675,0.941)
External Validation Set	0.890(0.794,0.985)	0.714(0.576,0.822)	0.594(0.423,0.745)	0.941(0.730,0.990)	0.950(0.764,0.991)	0.552(0.376,0.716)

Abbreviations: AUC, the area under the receiver operating characteristic curve; PPV, positive predictive value; NPV, negative predictive value

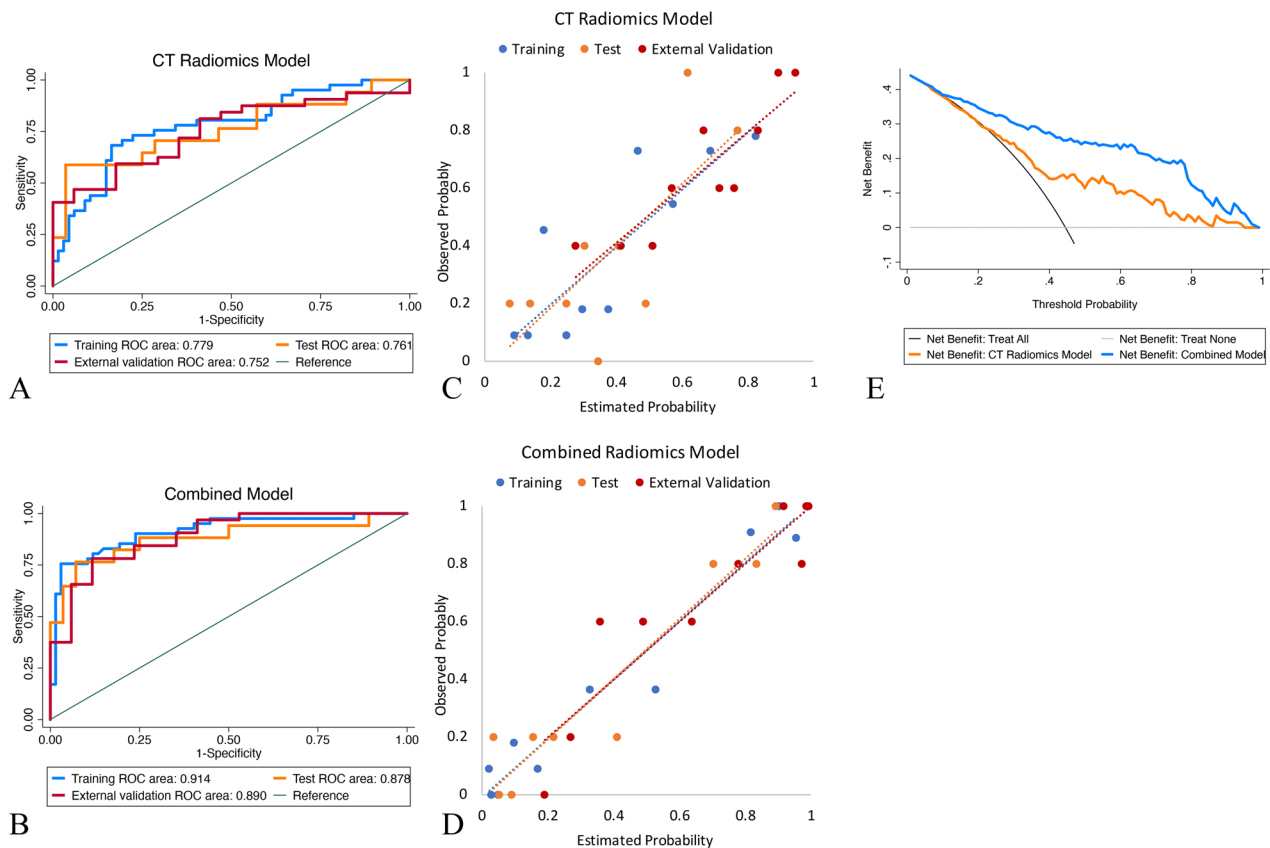


Fig. 3 Performance of the radiomics models for predicting microvascular invasion. Receiver operating characteristic (ROC) curve analysis for the training set, the test set and the external validation set showed that the combined model (B) had a higher area under the ROC curve than the CT radiomics model (A). Calibration curves for the training set, the test set and the external validation set showed that both the CT radiomics model (C) and the combined model (D) had strong consistency between estimated probability and observed probability. Decision curve analysis (E) indicated that the combined model was more beneficial for patients than the CT radiomics model

performance, indicating that integrating a full range of information is important for MVI prediction. Furthermore, some studies focused on MVI in HCC ≤ 5 cm, and the AUCs of the combined radiomics model in the external validation set or the test set were 0.74–0.858 [24–26]. Tian, YQ et al. used enhanced MRI radiomics-based nomogram to preoperatively predict MVI in HCC ≤ 3 cm, and the external validation AUC was 0.934 [27]. We only included HCC ≥ 3 cm in this study, and there are few studies focusing on MVI prediction in HCC ≥ 3 cm. We assume that limiting the lesion size within a certain range might contribute to the improvement of the radiomics models' performance, and future work is needed to verify this hypothesis.

Ultrasound features including color Doppler flow, maximal elasticity of HCCs, and maximal elasticity of the periphery of HCCs were significantly different between MVI (+) HCCs and MVI (-) HCCs [28]. However, there is room for improvement in the prediction performance of nomogram based on multi-modal ultrasound with AUC of 0.789 [29]. Zhang, R et al. used a new dynamic radiomics method based on dynamic

contrast-enhanced-MRI for predicting MVI in HCC. The dynamic radiomics had an improved effect on the MVI prediction in HCC with AUC of 0.777, compared with the static dynamic contrast-enhanced-MRI-based radiomics models [23]. Chen, YD et al. constructed a radiomics-based nomogram to predict MVI of small HCC. The AUC of hepatobiliary phase and diffusion-weighted imaging were 0.801–0.970 [30]. Although MRI has advantages in some aspects compared to CT, such as early diagnosis of HCC, the performance in MVI prediction of CT radiomics model is no worse than that of MRI radiomics model. 18 F-FDG PET metabolic and volumetric parameters were significant factors for predicting MVI in HCC [31, 32]. The hypermetabolic bright signal in PET can provide complements to the structural information in CT, and combining PET and CT can improve the performance of the model [33].

It is noted that the high-risk group predicted by the combined model, likely indicative of MVI, was associated with early intrahepatic recurrence and extrahepatic metastasis, indicating its potential application value in clinical decision-making. The same as previous studies,

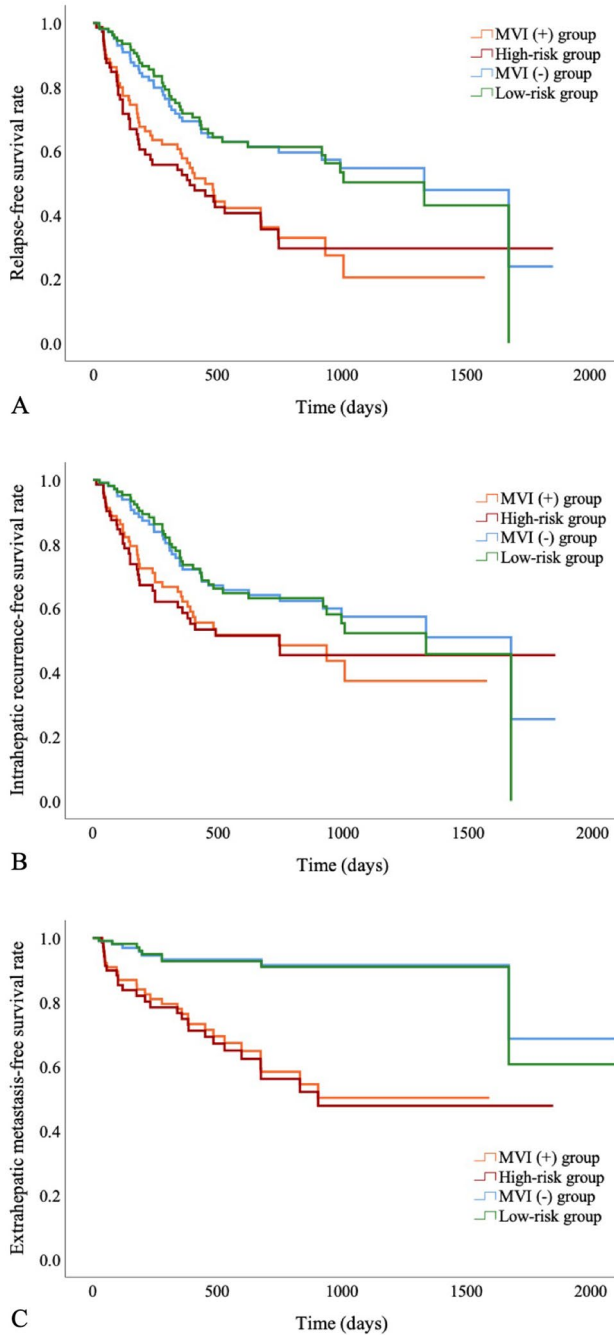


Fig. 4 Kaplan-Meier analysis of relapse-free survival. **(A)** Kaplan-Meier analysis of relapse-free survival rates according to combined model score and histopathology. **(B)** Kaplan-Meier analysis of intrahepatic recurrence-free survival rates according to combined model score and histopathology. **(C)** Kaplan-Meier analysis of extrahepatic metastasis-free survival rates according to combined model score and histopathology

MVI is an independent predictor for RFS after surgical resection. Compared to research by Hui Zhao et al. [34], in which the 1-, 3-year recurrence-free survival rates of MVI (+) and MVI (-) in HCC ≤ 5 cm were 72.4%, 47.8%, 81.4% and 60.6%, respectively, MVI (+) group showed

shorter recurrence-free survival in HCC ≥ 3 cm than in HCC ≤ 5 cm, and the difference of RFS between MVI (+) and MVI (-) was more obvious in HCC ≥ 3 cm. In clinical scenario, patients, who were classified into the high-risk group predicted by the combined model preoperatively, may undergo aggressive treatment and close surveillance.

SVM was used as a feature classifier in our study, and showed great contribution to the model performance. Consistent with previous studies, ML based radiomics enabled the integration and analyses of a large number of radiomics features to build a classification model for diagnosis or prediction [35, 36]. However, which ML method is the best to predict MVI based on CT radiomics is open to debate. Famularo et al. constructed a predictive CT radiomics model to assess the MVI status using 3 different supervised machine-learning algorithms (random-forest, fully connected MLP artificial neural network and extreme gradient boosting), and random-forest was the best performer with accuracy of 96.8% [37]. Xiong, L et al. constructed 12 CT radiomics models for MVI prediction using 3 modeling methods (logistic regression, support vector machine and Bayes) and 4 phase CT images (unenhanced phase, artery phase, portal venous phase and delay phase), and the logistic regression model with the artery phase radiomics signature showed the best performance with AUC of 0.848 [35]. Future work is needed to explore the optimal ML methods for feature selection and classification in terms of certain clinical problem and images [38].

All 13 radiomics features selected for the combined model are higher-order features, representing internal heterogeneity, and might be a result of the combination of blood vessels with abnormal hyperplasia, necrosis due to fast tumor growth, and uneven microenvironment of tumor [39]. In addition, despite different feature selector and classifier, several features selected for the radiomics model are consistent with previous studies, such as *glszm_SizeZoneNonUniformity* and *gldm_ClusterShade* [24, 40], indicating significant connections between these features and MVI. Furthermore, the selected features for the combined model, such as shape, capsule, peritumoral enhancement, internal arteries, hypodense halo and tumor-liver difference have been reported to predict MVI in several previous studies [9, 16]. To improve inter-observer agreement, which was fair to moderate in previous studies [41], the radiologists were trained through a number of cases before evaluating radiological features. It turns out that some features show good inter-observer reproducibility, such as diameter, shape, necrosis, peritumoral enhancement, internal arteries and hypodense halo. However, other features, such as border, capsule and tumor-liver difference, show moderate inter-observer reproducibility, which needs to be further improved in future studies. Besides, the same as previous studies, AFP

and ALB were integrated in the combined model indicating its predictive potential in MVI and RFS [21].

The study has some limitations. First, this was a retrospective study at a single institution. Further prospective study with patients collected from multiple centers is warranted. Second, there is a lack of interpretability of radiomics features at the biological level, and future work is needed to improve feature interpretability. Third, the inter-observer reproducibility needs to be improved. Fourth, manual extraction of VOI was used, which need extra labor and time cost. Future work is needed to integrate automatic segmentation and radiomics models.

Conclusions

In this study, we developed and validated two ML based radiomics models to noninvasively predict MVI and RFS in patients with HCC ≥ 3 cm preoperatively. Importantly, the high-risk group predicted by the combined model has shorter RFS. The combined model may serve as a noninvasive predictor and aid in clinical decision-making.

Abbreviations

HCC	Hepatocellular carcinoma
MVI	Microvascular invasion
RFS	Relapse-free survival
ML	Machine learning
SVM	Support vector machines
AFP	α -fetoprotein
PT	Prothrombin time
ALT	Alanine transaminase
AST	Aspartate transaminase
HBV DNA	Hepatitis B virus DNA
VOI	Volume of interest
ANOVA	Analysis of variance
ROC	Receiver operating characteristic
DCA	Decision curve analysis
AUC	Area under the ROC curve
PPV	Positive predictive value
NPV	Negative predictive value

Acknowledgements

Not Applicable

Author contributions

1 guarantor of integrity of the entire study: Jinan Wang, Xin Yue 2 study concepts and design: Xiaoli Zheng, Jinan Wang, Xin Yue 3 literature research: Hua Zhong, Yan Zhang, Xiaoli Zheng, Xin Yue 4 clinical studies: Hua Zhong, Yan Zhang, Guanbin Zhu, Jianghe Kang 5 experimental studies / data analysis: Hua Zhong, Yan Zhang, Guanbin Zhu, Ziyang Lin 6 statistical analysis: Hua Zhong, Yan Zhang, Guanbin Zhu, Ziyang Lin 7 manuscript preparation: Yan Zhang, Guanbin Zhu, Ziyang Lin 8 manuscript editing: Hua Zhong, Xiaoli Zheng, Jianghe Kang, Xin Yue.

Funding

This study has received funding by The Natural Science Foundation of Fujian Province [2023J011597].

Data availability

The data that support the findings of this study are not openly available and are available from the corresponding author upon reasonable request.

Declarations

Ethics approval and consent to participate

Ethical approval was obtained for this retrospective study from Institutional Review Board of Zhongshan Hospital of Xiamen University [2022(212)]. Written informed consent was waived by the Institutional Review Board of Zhongshan Hospital of Xiamen University. The study has been performed in accordance with the Declaration of Helsinki.

Consent for publication

Not Applicable

Clinical trial number

Not Applicable

Competing interests

The authors declare no competing interests.

Author details

¹Department of Radiology, Zhongshan Hospital of Xiamen University, School of Medicine, Xiamen University, No.201-209 Hubinnan Road, Siming District, Xiamen, Fujian Province 361004, China

²The Second Department of Radiology, The Second Affiliated Hospital of Xiamen Medical College, Xiamen, Fujian Province 361021, China

Received: 10 February 2025 / Accepted: 15 April 2025

Published online: 01 May 2025

References

- Toh MR, Wong EYT, Wong SH, et al. Global epidemiology and genetics of hepatocellular carcinoma. *article. Gastroenterology*. 2023;164(5):766–82. <https://doi.org/10.1053/j.gastro.2023.01.033>.
- Samant H, Amiri HS, Zibari GB. Addressing the worldwide hepatocellular carcinoma: epidemiology, prevention and management. *Review. J Gastrointest Oncol*. 2021;12:S361–S373. <https://doi.org/10.21037/jgo.2020.02.08>.
- Zhou J, Sun HC, Wang Z, et al. Guidelines for the diagnosis and treatment of hepatocellular carcinoma (2019 edition). *Article Liver Cancer*. 2020;9(6):682–720. <https://doi.org/10.1159/000509424>.
- Chen ZH, Zhang XP, Wang H, et al. Effect of microvascular invasion on the postoperative long-term prognosis of solitary small HCC: a systematic review and meta-analysis. *Review HPB (Oxford)*. 2019;21(8):935–44. <https://doi.org/10.1016/j.hpb.2019.02.003>.
- Zhang EL, Cheng Q, Huang ZY, et al. Revisiting surgical strategies for hepatocellular carcinoma with microvascular invasion. *Review Front Oncol*. 2021;11:1.691354. <https://doi.org/10.3389/fonc.2021.691354>.
- Lee HA, Lee YS, Kim BK, et al. Change in the recurrence pattern and predictors over time after complete cure of hepatocellular carcinoma. *Gut Liver*. 2021;15(3):420–29. <https://doi.org/10.5009/gnl20101>.
- Xu PJ, Zeng MS, Liu K, et al. Microvascular invasion in small hepatocellular carcinoma: is it predictable with preoperative diffusion-weighted imaging? *Article. J Gastroenterol Hepatol*. 2014;29(2):330–36. <https://doi.org/10.1111/jgh.12358>.
- Wang WT, Yang L, Yang ZX, et al. Assessment of microvascular invasion of hepatocellular carcinoma with diffusion kurtosis imaging. *Article. Radiology*. 2018;286(2):571–80. <https://doi.org/10.1148/radiol.2017170515>.
- Wang HH, Lu Y, Liu RK, et al. A non-invasive nomogram for preoperative prediction of microvascular invasion risk in hepatocellular carcinoma. *Article. Front Oncol*. 2021;11:13.745085. <https://doi.org/10.3389/fonc.2021.745085>.
- Zhu F, Yang F, Li J, et al. Incomplete tumor capsule on preoperative imaging reveals microvascular invasion in hepatocellular carcinoma: a systematic review and meta-analysis. *Rev Abdom Radiol*. 2019;44(9):3049–57. <https://doi.org/10.1007/s00261-019-02126-9>.
- Banerjee S, Wang DS, Kim HJ, et al. A computed tomography radiogenomic biomarker predicts microvascular invasion and clinical outcomes in hepatocellular carcinoma. *Article. Hepatology*. 2015;62(3):792–800. <https://doi.org/10.1002/hep.27877>.
- Gillies RJ, Kinahan PE, Hricak H. Radiomics: images are more than pictures, they are data. *Radiology*. 2016;278(2):563–77. <https://doi.org/10.1148/radiol.2015151169>.

13. Xia TY, Zhou ZH, Meng XP, et al. Predicting microvascular invasion in hepatocellular carcinoma using CT-based radiomics model. *Article. Radiology*. 2023;307(4):11. <https://doi.org/10.1148/radiol.222729>.
14. Reig B, Heacock L, Geras KJ, et al. Machine learning in breast MRI. *Review. J Magn Reson Imaging*. 2020;52(4):998–1018. <https://doi.org/10.1002/jmri.26852>.
15. Senturk ZK. Early diagnosis of Parkinson's disease using machine learning algorithms. *Article. Med Hypotheses*. 2020;138: 5.109603. <https://doi.org/10.1016/j.mehy.2020.109603>.
16. Renzulli M, Brocchi S, Cucchetti A, et al. Can current preoperative imaging be used to detect microvascular invasion of hepatocellular carcinoma? *Article. Radiology*. 2016;279(2):432–42. <https://doi.org/10.1148/radiol.2015.150998>.
17. Cong WM, Bu H, Chen J, et al. Practice guidelines for the pathological diagnosis of primary liver cancer: 2015 update. *Article World J Gastroenterol*. 2016;22(42):9279–87. <https://doi.org/10.3748/wjg.v22.i42.9279>.
18. Liu JB, Kuang SW, Zheng YL, et al. Prognostic and predictive significance of the tumor microenvironment in hepatocellular carcinoma. *Article. Cancer Biomark*. 2021;32(1):99–110. <https://doi.org/10.3233/cbm-203003>.
19. Yushkevich PA, Piven J, Hazlett HC, et al. User-guided 3D active contour segmentation of anatomical structures: significantly improved efficiency and reliability. *Article. Neuroimage*. 2006;31(3):1116–28. <https://doi.org/10.1016/j.neuroimage.2006.01.015>.
20. Song Y, Zhang J, Zhang YD, et al. FeAture explorer (FAE): a tool for developing and comparing radiomics models. *Article*. 2020;15(8):10.e0237587. *PLoS One*. <https://doi.org/10.1371/journal.pone.0237587>.
21. Zhang XM, Ruan SJ, Xiao WB, et al. Contrast-enhanced CT radiomics for preoperative evaluation of microvascular invasion in hepatocellular carcinoma: a two-center study. *Clin Transl Med*. 2020;102.
22. Xu TF, Ren LY, Liao MJ, et al. Preoperative radiomics analysis of contrast-enhanced CT for microvascular invasion and prognosis stratification in hepatocellular carcinoma. *Article. J Hepatocell Carcinoma*. 2022;9:189–201.
23. Zhang R, Wang Y, Li Z, et al. Dynamic radiomics based on contrast-enhanced MRI for predicting microvascular invasion in hepatocellular carcinoma. *BMC Med Imaging*. 2024;24(1, 80). <https://doi.org/10.1186/s12880-024-01258-9>
24. Liu P, Tan XZ, Zhang T, et al. Prediction of microvascular invasion in solitary hepatocellular carcinoma ≤ 5 cm based on computed tomography radiomics. *Article World J Gastroenterol*. 2021;27(17):2015–24. <https://doi.org/10.3748/wjg.v27.i17.2015>.
25. Wang F, Cheng M, Du BB, et al. Use of radiomics containing an effective peritumoral area to predict early recurrence of solitary hepatocellular carcinoma ≤ 5 cm in diameter. *Front Oncol*. 2022;121032115. <https://doi.org/10.3389/fonc.2022.1032115>.
26. Feng B, Wang LY, Zhu YJ, et al. The value of LI-RADS and radiomic features from MRI for predicting microvascular invasion in hepatocellular carcinoma within 5 cm. *Acad Radiol*. 2024;31(6):2381–90. <https://doi.org/10.1016/j.acra.2023.12.007>.
27. Tian YQ, Hua H, Peng QQ, et al. Preoperative evaluation of Gd-EOB-DTPA-enhanced MRI radiomics-based nomogram in small solitary hepatocellular carcinoma (≤ 3 cm) with microvascular invasion: a two-center study. *J Magn Reson Imaging*. 2022;56(5):1459–72. <https://doi.org/10.1002/jmri.28157>.
28. Jiang D, Qian Y, Tan BB, et al. Preoperative prediction of microvascular invasion in hepatocellular carcinoma using ultrasound features including elasticity. *World J Gastrointest Surg*. 2023;15(9):2042–51. <https://doi.org/10.4240/wjgs.v15.i9.2042>.
29. Zhong X, Peng JY, Xie YH, et al. A nomogram based on multi-modal ultrasound for prediction of microvascular invasion and recurrence of hepatocellular carcinoma. *Eur J Radiol* 2022;151110281. <https://doi.org/10.1016/j.ejrad.2022.110281>.
30. Chen YD, Zhang L, Zhou ZP, et al. Radiomics and nomogram of magnetic resonance imaging for preoperative prediction of microvascular invasion in small hepatocellular carcinoma. *World J Gastroenterol*. 2022;28(31):4399–416. <https://doi.org/10.3748/wjg.v28.i31.4399>.
31. Jiang CJ, Ma G, Liu QF, et al. The value of preoperative 18F-FDG PET metabolic and volumetric parameters in predicting microvascular invasion and postoperative recurrence of hepatocellular carcinoma. *Nucl Med Commun*. 2022;43(1):100–07. <https://doi.org/10.1097/mnm.0000000000001478>.
32. Jiang SP, Gao XQ, Tian YL, et al. The potential of 18F-FDG PET/CT metabolic parameter-based nomogram in predicting the microvascular invasion of hepatocellular carcinoma before liver transplantation. *Abdom Radiol*. 2024;49(5):1444–55. <https://doi.org/10.1007/s00261-023-04166-8>.
33. Ye ZJ, Zhang J, Wu N, et al. PET-guided attention for prediction of microvascular invasion in preoperative hepatocellular carcinoma on PET/CT. *Ann Nucl Med Apr*. 2023;37(4):238–45. <https://doi.org/10.1007/s12149-023-01822-3>.
34. Zhao H, Hua Y, Lu ZH, et al. Prognostic value and preoperative predictors of microvascular invasion in solitary hepatocellular carcinoma ≤ 5 cm without macrovascular invasion. *Oncotarget*. 2017;8(37):61203–14. <https://doi.org/10.18632/oncotarget.18049>.
35. Xiong L, Peng Y, Li S, et al. Machine learning-based radiomics for preoperative prediction of microvascular invasion in hepatocellular carcinoma. *Int J Radiat Res*. 2023;21(3):383–90. <https://doi.org/10.52547/ijrr.21.3.5>.
36. Chen W, Zhang T, Xu L, et al. Radiomics analysis of contrast-enhanced CT for hepatocellular carcinoma Grading. *Front Oncol*. 2021;11660509. <https://doi.org/10.3389/fonc.2021.660509>.
37. Famularo S, Penzo C, Maino C, et al. Preoperative detection of hepatocellular carcinoma's microvascular invasion on CT-scan by machine learning and radiomics: a preliminary analysis. *Ejsso*. 2025;51(1):108274. <https://doi.org/10.1016/j.ejsso.2024.108274>.
38. Wang XH, Wan Q, Chen HJ, et al. Classification of pulmonary lesion based on multiparametric MRI: utility of radiomics and comparison of machine learning methods. *Article Eur Radiol*. 2020;30(8):4595–605. <https://doi.org/10.1007/s00330-020-06768-y>.
39. Yao WJ, Yang S, Ge YQ, et al. Computed tomography radiomics-based prediction of microvascular invasion in hepatocellular carcinoma. *Article. Front Med*. 2022;9:10.819670. <https://doi.org/10.3389/fmed.2022.819670>.
40. Lv K, Cao X, Du P, et al. Radiomics for the detection of microvascular invasion in hepatocellular carcinoma. *Review. World J Gastroenterol*. 2022;28(20):2176–83. <https://doi.org/10.3748/wjg.v28.i20.2176>.
41. Min JH, Lee MW, Park HS, et al. Interobserver variability and diagnostic performance of gadoteric acid-enhanced MRI for predicting microvascular invasion in hepatocellular carcinoma. *Article. Radiology*. 2020;297(3):573–81. <https://doi.org/10.1148/radiol.2020201940>.

Publisher's Note

Springer Nature remains neutral with regard to jurisdictional claims in published maps and institutional affiliations.